

## First Test of Long-Range Collisional Drag via Plasma Wave Damping

M. Affolter, F. Anderegg, D. H. E. Dubin, and C. F. Driscoll

*Department of Physics, University of California at San Diego, La Jolla, California 92093, USA*

(Received 10 August 2016; published 4 October 2016)

This paper presents the first experimental confirmation of a new theory predicting enhanced drag due to long-range collisions in a magnetized plasma. The experiments measure damping of Langmuir waves in a multispecies pure ion plasma, which is dominated by interspecies collisional drag in certain regimes. The measured damping rates in these regimes exceed classical predictions of collisional drag damping by as much as an order of magnitude, but agree with the new theory.

DOI: [10.1103/PhysRevLett.117.155001](https://doi.org/10.1103/PhysRevLett.117.155001)

Collision rates are fundamental to our understanding of transport phenomena in plasmas. In magnetized plasmas, the classical theory of collisions [1–3] has long been used to describe these phenomena. However, when the cyclotron radius  $r_c \equiv q_s B / M_s c$  is less than the Debye length  $\lambda_D \equiv (T / 4\pi n_0 q_s^2)^{1/2}$ , it is known that classical theory is incomplete, since this theory neglects long-range collisions with impact parameters  $\rho$  in the range  $r_c < \rho < \lambda_D$  for which no parallel-perpendicular velocity scattering occurs. Here,  $B$  represents the magnetic field strength,  $q_s$  and  $M_s$  are the species charge and mass,  $n_0$  is the plasma density, and  $T$  is the plasma temperature in units of energy. Previous experiments and theory have shown that these long-range collisions enhance cross-field diffusion [4,5], heat transport [6,7], and viscosity [8,9] by orders of magnitude over classical theory when  $\lambda_D > r_c$ . The effect of long-range collisions on frictional drag was also considered theoretically using Fokker-Planck theory [10] and a Boltzmann analysis [11], but these theories are inconsistent, and in any case have never been tested.

A new theory [12] of long-range collisions resolves the inconsistencies, and predicts strongly enhanced parallel drag in magnetized plasmas for which  $\lambda_D > r_c$ . A new fundamental length scale  $d \equiv b(\bar{v}^2 / b^2 \nu_{ss'}^2)^{1/5} \propto T^{1/5}$  is identified in this theory, where  $b = q_s^2 / T$  is the distance of closest approach,  $\bar{v}$  is the thermal velocity, and  $\nu_{ss'}$  is the collision rate. This new length scale  $d$  separates long-range collisions into two regimes: (1)  $\rho < d$  where the colliding particles can be treated as a *correlated* sequence of two-body, pointlike, energy and momentum-conserving “Boltzmann” collisions and (2)  $\rho > d$  where multiple weak collisions occur simultaneously and Fokker-Planck analysis is valid. The long-range collisional enhancement of parallel drag applies to Penning trap plasmas for both matter and antimatter [13–15], for some astrophysical plasmas [16], and even for the edge region of tokamak plasmas [17–19].

Here we present the first experimental confirmation of this enhanced collisional drag, obtained through measurements of the damping of Langmuir waves in a multispecies

ion plasma. Collisional drag damping theory predicts damping proportional to the collisional interspecies parallel drag force. The measured damping rates are in quantitative agreement with the theory only when long-range collisions are included, since the enhanced parallel slowing rates exceed classical slowing rates from short-range collisions (with  $\rho < r_c$ ) by as much as an order of magnitude.

These damping measurements extend over a range of two decades in temperature where collisional drag damping is dominant. In this temperature range, the damping is dependent on the plasma composition and scales roughly as  $T^{-3/2}$ . At higher temperatures, Landau damping dominates, and at lower temperatures centrifugal mass separation [20–23] and collisional locking of the fluid elements becomes significant. At ultralow temperatures, the plasma approaches the moderately coupled regime, and these damping measurements may provide insight into the collisionality of a correlated, magnetized plasma.

A cylindrical Penning-Malmberg trap is used to confine these multispecies ion plasmas [24], with  $B_z = 3$  Tesla. The ions are predominately  $\text{Mg}^+$  from a Magnesium vacuum electrode arc, with 5%–30% impurity ions, consisting mostly of  $\text{H}_3\text{O}^+$ , from chemical reactions with the background gas. The impurity ion fraction is varied by changing the background gas pressure over the range  $10^{-10} \leq P \leq 10^{-8}$  Torr.

A quantitative determination of the species fraction  $\delta_s$  and mass  $M_s$  for each species  $s$  is obtained by measuring the resulting heating from short, resonant cyclotron bursts (200–800 cycles) [23]. The charge fractions are measured to a 10% accuracy down to a  $\delta_s \sim 0.5\%$  level. A typical “dirty” plasma composition consists of the three naturally occurring Magnesium isotopes (24, 25, and 26),  $\text{H}_3\text{O}^+$  (19),  $\text{HCO}^+$  (29),  $\text{O}_2^+$  (32),  $\text{C}_3\text{H}_3^+$  (39), and  $\text{C}_3\text{H}_7^+$  (43), with  $\delta_s \sim (52, 9, 10, 16, 4, 4, 4, 1)\%$ , respectively.

By using a weak applied “rotating wall” (RW) field [25], these cylindrical ion plasmas are confined for days in a near thermal equilibrium state described by “top-hat” density and rigid-rotor rotation profiles. Radial profiles of the total  $\text{Mg}^+$  density, rotation velocity, and plasma temperature are measured through laser induced fluorescence

(LIF) techniques [24]. A typical plasma has a radius  $R_p \sim 0.5$  cm, density  $n_0 \sim 1.9 \times 10^7$  cm $^{-3}$ , length  $L_p \sim 10$  cm, and rotates at  $f_E \sim 9$  kHz. Altering the frequency of the RW enables control of the rotation rate  $f_E = (4 \rightarrow 31)$  kHz and thus the plasma density  $n_0 = (0.9 \rightarrow 6.4) \times 10^7$  cm $^{-3}$ .

The plasma temperature  $T$  is controlled from  $10^{-4}$  to 1 eV through laser cooling of the  $^{24}\text{Mg}^+$  ions. This enables damping measurements spanning regimes from collisionless Landau damping to collisional drag damping. For plasmas at  $T \gtrsim 10^{-3}$  eV (11.6 Kelvin), the ions species are uniformly mixed. In contrast, at  $T < 10^{-3}$  eV, the species begin to centrifugally separate by mass [20–23], with near-complete separation at  $T < 10^{-4}$  eV.

The damping measurements are performed on azimuthally symmetric, standing plasma (Langmuir) waves. In these radially bounded plasmas, the wave frequencies are near-acoustic, because of the shielding of the cylindrical confinement electrodes at a radius  $R_w = 2.86$  cm. This Trivelpiece-Gould (TG) dispersion relation [26] for azimuthally symmetric modes is approximately

$$f_{\text{TG}} = f_p \frac{k_z}{\sqrt{k_z^2 + k_\perp^2}} \left[ 1 + \frac{3}{2} \left( \frac{\bar{v}}{v_{ph}} \right)^2 \right], \quad (1)$$

where  $k_z \equiv m_z \pi / L_p$  and  $k_\perp = R_p^{-1} [2 / \ln(R_w / R_p)]^{1/2}$  are the axial and transverse wave numbers, respectively, and  $f_p$  is the plasma frequency.

These waves are excited with a rf burst at the linear mode frequency applied to an end confinement ring, and they are detected on a confinement ring located slightly off of the plasma center. Typically, a 10 cycle sine wave burst with a 5 mV $_{\text{pp}}$  amplitude is used, resulting in a wave density perturbation  $\delta n / n_0 \sim 0.5\%$ , and wave fluid velocity  $v_f \sim 20$  m/s, with a concomitant heating of the plasma by about  $3 \times 10^{-5}$  eV. For this work, we investigate the damping of the lowest order  $m_z = 1$  axial mode occurring at a frequency  $f_1 \sim 26$  kHz, with phase velocity  $v_{ph} = 5200$  m/s compared to thermal velocity  $\bar{v} = 63$  m/s at  $T = 10^{-3}$  eV.

The time evolution of the wave amplitude, as shown in Fig. 1, is obtained through sine wave fits to the detected wave signal in time segments of approximately 5 wave cycles. An exponential fit to this decreasing wave amplitude determines the damping rate  $\gamma$ . At  $T = 2.7 \times 10^{-3}$  eV, a typical damping rate is  $\gamma \sim 132$  s $^{-1}$  for a “dirty” plasma composition.

Figure 2 shows measurements of the damping rate over four decades in the plasma temperature. At high temperatures ( $T \sim 0.5$  eV), collisionless Landau damping dominates. Quantitative agreement with Landau theory is obtained for small amplitude waves as indicated by the solid red curve [27]. This prototypical Landau damping becomes exponentially weak for  $T \lesssim 0.2$  eV. However, we

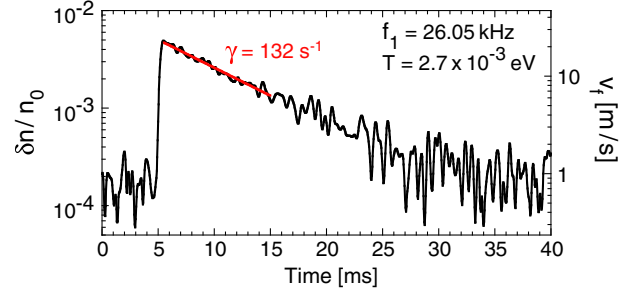


FIG. 1. The amplitude evolution of an  $m_z = 1$  TG wave. An exponential fit (red curve) to the decreasing amplitude determines the damping rate. The measured mode frequency remains constant over the evolution.

believe that Landau damping is extended to a lower temperature regime ( $0.02 \lesssim T \lesssim 0.2$  eV) through the same Landau interaction acting on “bounce-harmonics” of the wave introduced through finite-length effects. At present, the harmonics introduced from the plasma ends are ill understood, but recent experiments [28] with controlled harmonic generation have shown stronger damping in good agreement with bounce harmonic damping theory [29] in this temperature regime.

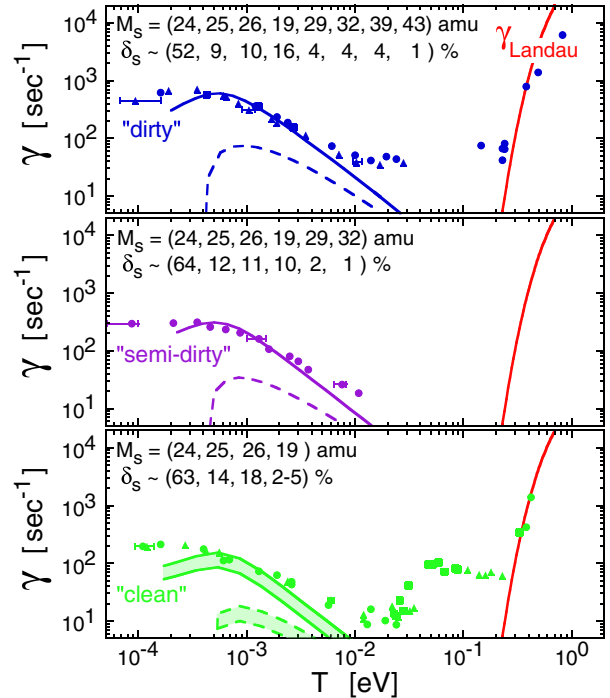


FIG. 2. Symbols are damping measurements on plasmas with three different species compositions and a density  $n_0 \sim 1.9 \times 10^7$  cm $^{-3}$ . Symbol shapes represent measurements on different plasmas. Curves correspond to drag damping predictions for both a classical calculation that assumes only short-range collisions (dashed), and a calculation including the new long-range enhanced collisional slowing (solid). Horizontal error bars represent typical radial variations in the temperature. Vertical errors are smaller than the symbol size.

Here, we focus on  $T \lesssim 10^{-2}$  eV, where the damping is dependent on the plasma composition, and scales roughly as  $T^{-3/2}$ . Figure 2 shows damping measurements on plasmas with three different compositions. We find that the damping increases by a factor of 4 as the concentration of impurities is increased from the “clean” to “dirty” plasma compositions. The uncertainty in the measured damping rates is about  $\pm 10\%$ , which is smaller than the vertical size of the symbols. The scatter of the different symbol shapes for a given composition corresponds to damping measurements on different plasmas with slight compositional variations, but roughly the same damping. For  $T \lesssim 10^{-3}$  eV, the damping is observed to decrease from the  $T^{-3/2}$  scaling, consistent with the onset of centrifugal mass separation. The fact that the measured damping is dependent on the plasma composition and scales as  $T^{-3/2}$  supports interspecies drag as the observed damping mechanism.

This interspecies drag damping is adequately modeled by cold fluid theory. Basically, ions are accelerated by the wave electric field as  $q_s E/M_s$ , producing a disparity in the velocity of different species. Interspecies collisions then cause drag forces on each species, which damps the wave. The oscillating velocity  $v_f^{(s)}$  of species  $s$  parallel to the magnetic field is predicted to be

$$v_f^{(s)} = \frac{q_s k_z \delta\phi}{M_s \omega} - i \sum_{s'} \frac{\nu_{ss'}}{\omega} (v_f^{(s)} - v_f^{(s')}), \quad (2)$$

where  $\nu_{ss'}$  is the collisional slowing rate between species  $s$  and  $s'$ ,  $\delta\phi$  is the wave potential, and  $\omega$  is the complex wave frequency.

We are able to directly measure the mean velocities of the three  $\text{Mg}^+$  isotopes by measuring the parallel velocity distribution  $F(v_{\parallel})$  coherent with the wave-phase  $\theta_l(t)$  received on the wall. Figure 3 (top) shows the wave-phase coherent  $F(v_{\parallel})$  of the  $\text{Mg}^+$  isotopes for 8 different phase bins  $\theta_l = (l-1)2\pi/8$ . These wave-phase coherent distributions are measured by tuning the probe laser frequency to be resonant with a  $\text{Mg}^+$  isotope moving at a velocity  $v_{\parallel}$ . A wave is then excited, and the time of arrival of each fluorescent photon is recorded along with the wave amplitude and phase. The photons are then binned by wave phase over 400 wave cycles. This process is repeated at 512 different velocities (laser frequency detunings) to construct  $F(v_{\parallel})$ . The  $\text{Mg}^+$  distributions are found to oscillate around  $v = 0$  (vertical orange lines) as the ions are accelerated by the wave electric field. Here a large amplitude drive of 20 m V<sub>pp</sub> has been used to induce a fluid velocity  $v_f^{(24)} = 77$  m/s comparable to the thermal speed  $\bar{v}$ .

The black symbols and curves in Fig. 3 (bottom) are measurements of and sine wave fits to the central velocity of each isotope distribution for the 8 different phase bins. These fits determine the oscillating fluid velocity of each

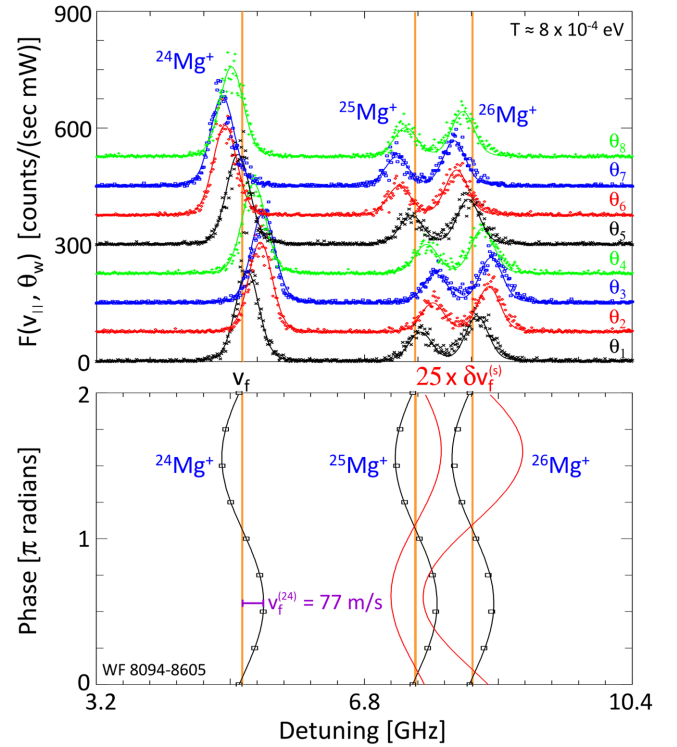


FIG. 3. Measurements of the parallel velocity distribution function  $F(v_{\parallel})$  coherent with the wave-phase  $\theta_l(t)$  (top); each phase is offset for clarity. Black symbols and curves (bottom) are measurements of and sine wave fits to the central velocity of the oscillating  $\text{Mg}^+$  distributions. Red curves (bottom) are  $25\times$  the relative velocity of the  $\text{Mg}^+$  isotopes to that of  $^{24}\text{Mg}^+$ .

$\text{Mg}^+$  isotope. The velocity difference  $\delta v_f^{(s)} \equiv v_f^{(s)} - v_f^{(24)}$  of the isotopes  $^{25}\text{Mg}^+$  and  $^{26}\text{Mg}^+$  are represented by the red curves. We find  $\delta v_f^{(25)} = -(4.1 \pm 1.1)\% v_f^{(24)}$  and  $\delta v_f^{(26)} = -(8.2 \pm 1.1\%) v_f^{(24)}$  in agreement with the 4% and 8% increases in the respective isotopic masses. That is, the species move independently in the (single) electric field, with weak collisional interactions.

The drag damping is calculated by solving for  $\omega \equiv \omega_r + i\gamma$  in the linearized Poisson equation,

$$\frac{1}{r} \frac{\partial}{\partial r} \left( r \frac{\partial \delta\phi}{\partial r} \right) - k_z^2 \delta\phi = -\frac{4\pi q_s k_z}{\omega} \sum_s n_{0s} v_f^{(s)} \quad (3)$$

using a shooting method. Here, the linearized continuity equation  $\delta n_s = k_z n_{0s} v_f^{(s)} / \omega$  has been used to replace the perturbed density  $\delta n_s$  with the species velocity  $v_f^{(s)}$ . Also, the equilibrium density  $n_{0s}$  has radial dependence at low temperatures when centrifugal mass separation becomes important.

For plasmas that are both radially uniform and have weak collisionality ( $\nu_{ss'} \ll \omega_{TG}$ ), the collisional drag damping can be solved analytically as

$$\gamma = \frac{1}{4\omega_p^2} \sum_s \sum_{s'} \frac{(M_{s'} - M_s)^2}{M_{s'}^2} \omega_{p,s}^2 \nu_{ss'}, \quad (4)$$

where  $\omega_{p,s}^2 = 4\pi q_s^2 n_{0s}/M_s$  is the species plasma frequency, and  $\omega_p^2 = \sum \omega_{p,s}^2$  is the total plasma frequency. This equation is valid in the regime  $T \gtrsim 10^{-3}$  eV for the plasmas considered in these experiments. Equation (4) recovers the electron-ion drag damping results of Lenard and Bernstein [30] for neutral plasmas. The enhancement of  $\nu_{ss'}$  due to long-range collisions will be seen to increase the drag damping.

Recent theory [12] has shown that two types of long-range collisions occur, separated by the newly identified diffusion scale length  $d \equiv b(\bar{v}^2/b^2\nu_{ss'}^2)^{1/5} \propto T^{1/5}$ . In these experiments, the diffusion scale length is varied over the range  $33 \lesssim d \lesssim 135 \mu\text{m}$  by changing the plasma temperature  $10^{-4} \lesssim T \lesssim 1$  eV. For impact parameters  $\rho < d$ , collisions occur faster than the diffusion time scale, so they can be regarded as isolated Boltzmann collisions. In contrast, for  $\rho > d$ , multiple weak collisions occur simultaneously and particles diffuse in velocity, so Fokker-Planck theory is required. The predicted slowing-down rate has the “classical” scaling  $\nu_{ss'} = \sqrt{\pi} n_{0s'} \bar{v}_{ss'} b^2 \ln \Lambda$ , where  $\bar{v}_{ss'} = \sqrt{2T\mu}/M_s$ ,  $\mu = M_s M_{s'}/(M_s + M_{s'})$  is the reduced mass, with an enhanced Coulomb logarithm

$$\ln \Lambda = \frac{4}{3} \ln \left( \frac{\min[r_c, \lambda_D]}{b} \right) + h \ln \left( \frac{d}{\max[b, r_c]} \right) + 2 \ln \left( \frac{\lambda_D}{\max[d, r_c]} \right). \quad (5)$$

The first logarithmic term in Eq. (5) is from classical short-range collisions and is equivalent to  $5\nu_{ii}/4$  [31]. The collisional slowing rate is enhanced by the second and third terms, which represent long-range Boltzmann and Fokker-Planck collisions, respectively. For repulsive (like-sign) collisions  $h = 5.899$ , increased from 4 due to “collisional caging” [4] whereas  $h = 0$  for attractive (opposite-sign) collisions in neutralized plasmas.

Predictions of the drag damping theory for both a classical calculation that assumes only short-range collisions (dashed line), and a calculation including the new long-range enhanced collisional slowing (solid line) are shown in Fig. 2. Theory is in quantitative agreement with the experimental results only when long-range collisions are included, since the slowing rates exceed classical short-range rates by as much as an order of magnitude. The broadness of the “clean” plasma theory curve results from a larger uncertainty in the species fractions.

At  $T \lesssim 10^{-3}$  eV, the measured and predicted drag damping rates decrease from the nominal  $T^{-3/2}$  scaling. Two effects are responsible for this decrease. First, the ions begin to centrifugally separate by mass, with the lighter ions near  $r = 0$ . This radial separation reduces the species

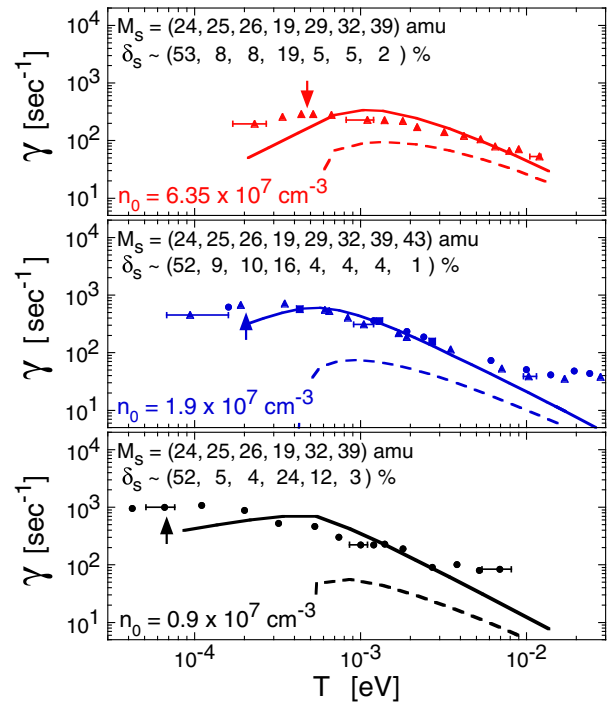


FIG. 4. Drag damping rates on three plasmas with different densities and compositions. Symbols are measurements and curves are theory predictions assuming only classical collisions (dashed line) or including long-range enhanced collisions (solid line). Arrows indicate the temperature of peak measured damping.

overlap, and thus reduces the interspecies drag. Secondly, the collision rates approach the wave frequency, so species collide before developing a disparity in velocity. In essence, the species fluid elements begin to collisionally lock, which decreases the drag.

Both fluid locking and centrifugal separation are dependent on the plasma density. Figure 4 focuses on the narrower temperature regime of drag damping for three different density plasmas. A similar quantitative agreement with long-range enhanced drag damping theory is observed as the density is changed by a factor of 7. As the density increases, centrifugal separation and fluid locking occur at higher temperatures, and a corresponding increase in the temperature of the measured “peak” damping is observed. These results suggest that fluid locking and centrifugal separation are at least in part responsible for the decrease in the damping from the  $T^{-3/2}$  scaling.

For  $T \lesssim 4 \times 10^{-4}$  eV, current theory is inadequate. Global correlation effects become significant, with correlation parameter  $\Gamma \equiv q_s^2/aT \gtrsim 0.2$  for  $n_0 = 1.9 \times 10^7 \text{ cm}^{-3}$  here  $a \equiv (3/4\pi n_0)^{1/3}$ . Correlations limit the parallel collisionality [32–34], decreasing the effects of fluid locking, and increasing the predicted damping rates. Also, in this centrifugally separated regime, viscosity from like-particle collisions [35] may be important, which is not included in the current theory.

In summary, measurements of collisional interspecies drag damping provide the first experimental confirmation of enhanced collisional slowing due to long-range collisions. Collisional drag damping theory is in quantitative agreement with the experimental results for a range of plasma compositions and densities only when long-range collisions are included. At low temperatures  $T \lesssim 10^{-3}$  eV, the observed damping is reduced from the typical  $T^{-3/2}$  collisional scaling as centrifugal separation and fluid locking become significant. Correlations and viscosity may increase the damping at ultralow temperatures.

This work was supported by NSF Grant No. PHY-1414570 and DOE Grant No. DE-SC0002451.

- 
- [1] L. Spitzer and R. Härm, *Phys. Rev.* **89**, 977 (1953); R. S. Cohen, L. Spitzer, and P. M. Routly, *Phys. Rev.* **80**, 230 (1950).
- [2] C. L. Longmire and M. N. Rosenbluth, *Phys. Rev.* **103**, 507 (1956).
- [3] M. N. Rosenbluth and A. N. Kaufman, *Phys. Rev.* **109**, 1 (1958).
- [4] D. H. E. Dubin, *Phys. Rev. Lett.* **79**, 2678 (1997).
- [5] F. Anderegg, X.-P. Huang, C. F. Driscoll, E. M. Hollmann, T. M. O’Neil, and D. H. E. Dubin, *Phys. Rev. Lett.* **78**, 2128 (1997).
- [6] D. H. E. Dubin and T. M. O’Neil, *Phys. Rev. Lett.* **78**, 3868 (1997).
- [7] E. M. Hollmann, F. Anderegg, and C. F. Driscoll, *Phys. Rev. Lett.* **82**, 4839 (1999).
- [8] C. F. Driscoll, J. H. Malmberg, and K. S. Fine, *Phys. Rev. Lett.* **60**, 1290 (1988).
- [9] J. M. Kriesel and C. F. Driscoll, *Phys. Rev. Lett.* **87**, 135003 (2001).
- [10] N. Rostoker, *Phys. Fluids* **3**, 922 (1960).
- [11] T. M. O’Neil, *Phys. Fluids* **26**, 2128 (1983).
- [12] D. H. E. Dubin, *Phys. Plasmas* **21**, 052108 (2014).
- [13] G. Andresen *et al.*, *Nature (London)* **468**, 673 (2010).
- [14] G. Gabrielse, X. Fei, L. A. Orozco, R. L. Tjoelker, J. Haas, H. Kalinowsky, T. A. Trainor, and W. Kells, *Phys. Rev. Lett.* **63**, 1360 (1989).
- [15] B. M. Jelenković, A. S. Newbury, J. J. Bollinger, W. M. Itano, and T. B. Mitchell, *Phys. Rev. A* **67**, 063406 (2003).
- [16] A. M. Beloborodov and C. Thompson, *Astrophys. J.* **657**, 967 (2007).
- [17] J. A. Boedo, D. L. Rudakov, R. A. Moyer, G. R. McKee, R. J. Colchin, M. J. Schaffer, P. Stangeby, W. West, S. L. Allen, T. E. Evans *et al.*, *Phys. Plasmas* **10**, 1670 (2003).
- [18] Y. Liang, H. Koslowski, P. Thomas, E. Nardon, B. Alper, P. Andrew, Y. Andrew, G. Arnoux, Y. Baranov, M. Bécoulet *et al.*, *Phys. Rev. Lett.* **98**, 265004 (2007).
- [19] B. LaBombard, J. Rice, A. Hubbard, J. Hughes, M. Greenwald, J. Irby, Y. Lin, B. Lipschultz, E. Marmor, C. Pitcher *et al.*, *Nucl. Fusion* **44**, 1047 (2004).
- [20] T. M. O’Neil, *Phys. Fluids* **24**, 1447 (1981).
- [21] G. Andresen *et al.*, *Phys. Rev. Lett.* **106**, 145001 (2011).
- [22] D. J. Larson, J. C. Bergquist, J. J. Bollinger, W. M. Itano, and D. J. Wineland, *Phys. Rev. Lett.* **57**, 70 (1986).
- [23] M. Affolter, F. Anderegg, D. H. E. Dubin, and C. F. Driscoll, *Phys. Plasmas* **22**, 055701 (2015).
- [24] F. Anderegg, X.-P. Huang, E. Sarid, and C. F. Driscoll, *Rev. Sci. Instrum.* **68**, 2367 (1997).
- [25] F. Anderegg, E. M. Hollmann, and C. F. Driscoll, *Phys. Rev. Lett.* **81**, 4875 (1998).
- [26] A. Trivelpiece and R. Gould, *J. Appl. Phys.* **30**, 1784 (1959).
- [27] J. R. Danielson, F. Anderegg, and C. F. Driscoll, *Phys. Rev. Lett.* **92**, 245003 (2004).
- [28] F. Anderegg, M. Affolter, A. A. Kabantsev, D. H. E. Dubin, A. Ashourvan, and C. F. Driscoll, *Phys. Plasmas* **23**, 055706 (2016).
- [29] A. Ashourvan and D. H. E. Dubin, *Phys. Plasmas* **21**, 052109 (2014).
- [30] A. Lenard and I. B. Bernstein, *Phys. Rev.* **112**, 1456 (1958).
- [31] T. M. O’Neil and C. F. Driscoll, *Phys. Fluids* **22**, 266 (1979).
- [32] G. Dimonte and J. Daligault, *Phys. Rev. Lett.* **101**, 135001 (2008).
- [33] S. D. Baalrud and J. Daligault, *Phys. Rev. Lett.* **110**, 235001 (2013).
- [34] G. Bannasch, J. Castro, P. McQuillen, T. Pohl, and T. C. Killian, *Phys. Rev. Lett.* **109**, 185008 (2012).
- [35] M. Anderson and T. O’Neil, *Phys. Plasmas* **14**, 112110 (2007).